Rapid Collapse into a Molten Globule Is Followed by Simple Two-State Kinetics in the Folding of Lysozyme from Bacteriophage λ

ARTICLE *in* BIOCHEMISTRY · OCTOBER 2010

Impact Factor: 3.02 · DOI: 10.1021/bi101126f · Source: PubMed

5 AUTHORS, INCLUDING:

Alexandre Di Paolo
University of Melbourne
6 PUBLICATIONS **39** CITATIONS
SEE PROFILE

Edwin De Pauw
University of Liège
391 PUBLICATIONS **7,201** CITATIONS
SEE PROFILE

Christina Redfield
University of Oxford
129 PUBLICATIONS **4,678** CITATIONS
SEE PROFILE

Andre Matagne
University of Liège
73 PUBLICATIONS **2,414** CITATIONS
SEE PROFILE

8646 *Biochemistry* **2010,** *49,* 8646–8657
DOI: 10.1021/bi101126f

BIOCHEMISTRY
including biophysical chemistry & molecular biology
Article

Rapid Collapse into a Molten Globule Is Followed by Simple Two-State Kinetics in the Folding of Lysozyme from Bacteriophage λ†

Alexandre Di Paolo,‡ Dorothée Balbeur,§ Edwin De Pauw,§ Christina Redfield,∥ and André Matagne*,‡

‡*Laboratoire d'Enzymologie et Repliement des Protéines, Centre d'Ingénierie des Protéines, and* §*Département de Chimie, Chimie Physique, Spectrométrie de Masse, Université de Liège, Institut de Chimie B6, 4000 Liège (Sart Tilman), Belgium, and* ∥*Department of Biochemistry, University of Oxford, South Parks Road, Oxford OX1 3QU, United Kingdom*

Received July 15, 2010; Revised Manuscript Received August 24, 2010

ABSTRACT: Stopped-flow fluorescence and circular dichroism spectroscopy have been used in combination with quenched-flow hydrogen exchange labeling, monitored by two-dimensional NMR and electrospray ionization mass spectrometry, to investigate the folding kinetics of lysozyme from bacteriophage λ (λ lysozyme) at pH 5.6, 20 °C. The first step in the folding of λ lysozyme occurs very rapidly ($\tau < 1$ ms) after refolding is initiated and involves both hydrophobic collapse and formation of a high content of secondary structure but only weak protection from $^1H/^2H$ exchange and no fixed tertiary structure organization. This early folding step is reflected in the dead-time events observed in the far-UV CD and ANS fluorescence experiments. Following accumulation of this kinetic molten globule species, the secondary structural elements are stabilized and the majority (ca. 88%) of refolding molecules acquire native-like properties in a highly cooperative two-state process, with $\tau = 0.15 \pm 0.03$ s. This is accompanied by the acquisition of substantial native-like protection from hydrogen exchange. A double-mixing experiment and the absence of a denaturant effect reveal that slow ($\tau = 5 \pm 1$ s) folding of the remaining (ca. 12%) molecules is rate limited by the *cis*/*trans* isomerization of prolines that are *trans* in the folded enzyme. In addition, native state hydrogen exchange and classical denaturant unfolding experiments have been used to characterize the thermodynamic properties of the enzyme. In good agreement with previous crystallographic evidence, our results show that λ lysozyme is a highly dynamic protein, with relatively low conformational stability ($\Delta G°_{N-U} = 25 \pm 2$ kJ·mol^{-1}).

Both virus (v-type) and eukaryotic (especially c-type) lysozymes have been used as model systems to study the mechanism of protein folding and the determinants of protein stability. Despite the lack of statistically significant sequence identity between enzymes from different classes, they all belong to the same superfamily of bacterial peptidoglycan hydrolases (*1*) and share clear structural similarities. In particular, all lysozymes display a pronounced two-domain structure, with the active site invariably situated in a deep cleft at the interface between the domains, which are distinctly connected by a helix. In all enzymes, a catalytically essential Glu is found in the active site at the C-terminal end of a helix, which is followed by a short multistranded β-sheet.

Hen egg white (129 residues) and T4 (164 residues) lysozymes have been studied in detail as typical representatives of the c- and v-type lysozymes, respectively. In particular, lysozyme from phage T4 and ca. 700 variants have been characterized by Matthews and co-workers (for a recent review, see ref *2*) in order to probe the factors that determine the structure and stability of proteins. Thermodynamic analysis of the wild-type and mutant T4 lysozymes has been based on a cooperative two-state model for folding (*3*). Native state hydrogen exchange studies (*4*) have demonstrated, however, that the two structural (sub)domains of T4 lysozyme behave as energetically independent units. Furthermore, detailed analysis of the kinetics of the folding reaction revealed the presence of two intermediate species, on both the unfolding and refolding sides of the rate-limiting transition state. Thus, analysis of several mutants at low temperature (*5*), pulse-labeling hydrogen exchange (*6*) and stopped-flow circular dichroism (CD) [1]combined with chevron plot analysis of the kinetics (*7*) provided evidence that T4 lysozyme refolds through an early intermediate. The existence of this species has, however, recently been called into question (*8*). On the other side of the transition barrier, another distinct partially folded (hidden) intermediate, with unfolded and folded N- and C-terminal domains (*4*, *9*), respectively, was detected by native state hydrogen exchange. Chevron plot analysis demonstrated significant population of this unfolding intermediate, at high denaturant concentrations, for many lysozyme variants (*4*).

In the case of hen lysozyme (*10*−*18*), despite the similar simple two-state equilibrium folding, refolding has been found to be a

†This work was supported in part by grants from the Fonds de la Recherche Fondamentale et Collective (contract numbers 2.4530.09, 2.4550.05, and 2.4614.10), by the Belgian program of Interuniversity Attraction Poles initiated by the Federal Office for Scientific Technical and Cultural Affairs (PAI number P6/19), and by the Wellcome Trust (grant number 079440). The FTMS was funded by the FEDER (contract number UR 12020000082-230008). A.M. is a Research Associate of the National Fund for Scientific Research (FRS-FNRS, Belgium). D.B. was a Research Fellow of the National Fund for Scientific Research (FRS-FNRS, Belgium). A.D.P. was recipient of a FRIA fellowship and was awarded short-term fellowships from the EMBO and the FRS-FNRS (Belgium) to support his stay in Oxford.

*To whom correspondence should be addressed. E-mail: amatagne@ulg.ac.be. Telephone: +32(0)43663419. Fax: +32(0)43663396.

[1]Abbreviations: ANS, 1-anilino-8-naphthalenesulfonate, CD, circular dichroism; ESI-MS, electrospray ionization mass spectrometry; GdmHCl, guanidinium chloride; HEPES, *N*-(2-hydroxyethyl)piperazine-*N*′-2-ethanesulfonic acid; HSQC, heteronuclear single-quantum coherence.

 Published on Web 08/31/2010

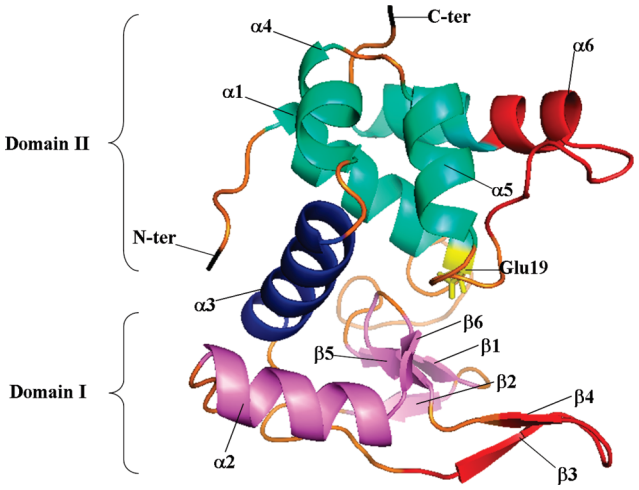

FIGURE 1: Schematic ribbon representation of the structure of λ lysozyme in its open conformation (1AM7 (*21*)). The secondary structure elements in domains I (β1−6 and α2) and II (α4−6 and α1) are shown in cyan and purple, respectively, and helix α3, which connects the two domains, is in blue. The catalytic Glu19 is shown in yellow, and the N- and C-terminal ends of the enzyme are indicated and colored black. The mobile regions observed in the crystal structure (i.e., 51−60 and 128−141; see text) are highlighted in red. The figure was drawn using the open-source molecular graphics system PyMOL.

complex process, with the following distinct features: (1) a heterogeneous kinetically collapsed state, with molten globule properties, is formed rapidly; (2) the two structural domains that make up the native state fold autonomously in ca. 70% of molecules and thus behave as distinct folding domains; (3) parallel folding events are observed in which acquisition of native-like hydrogen protection and formation of a competent active site occur with significantly different time constant values, i.e., ~100 and ~350 ms for the fast (~25%) and slow (~75%) populations of refolding molecules, respectively; (4) at least two distinct partially folded species are populated, which are productive on-pathway intermediates. In particular, a stable intermediate accumulates on the slow pathway, in which only the α-domain is persistently structured in the absence of a stable β-domain. Studies with hen lysozyme have provided important insights into the general mechanism of protein folding (*19*, *20*).

Lysozyme from bacteriophage λ (λ lysozyme) is a monomeric protein of 158 amino acid residues (17825 Da), which consists of ca. 51% regular secondary structure (42% helical and 9% β-sheet; Figure 1) organized in two domains (*21*, *22*). Domain I is composed of six β-strands, forming two β-sheets, and of one α-helix (α2). Domain II consists of four α-helices (α1, α4, α5, α6), whereas the remaining α3 helix serves as a link between the two domains. The enzyme displays open and closed conformations, with large structural differences in regions spanning residues 51−60 and 128−141 (*21*, *22*). In the closed conformation, β-strands β3 and β4 in domain I are disrupted, and this region of the protein forms a long loop which partially blocks access to the active site cavity. Furthermore, another loop in domain II, connecting helices α5 and α6, extends across the active site cleft and also restricts the access to the cavity. In common with other lysozymes, λ lysozyme catalyzes the cleavage of the β-1,4-glycosidic bond between *N*-acetylmuramic acid (MurNAc) and *N*-acetylglucosamine (GlcNAc) residues in the peptidoglycan of the bacterial cell wall. However, the mechanism (*23*) is different from that of other lysozymes; breakage of the β-1,4 bond between MurNAc and GlcNAc results in intramolecular transglycosylation and not in hydrolysis, as is usually the case. Remarkably, the fold of λ lysozyme resembles that of the glycosyltransferase domain of the peptidoglycan-synthesizing penicillin-binding proteins (PBPs) from *Staphylococcus aureus* (PBP2 (*24*)) and *Aquifex aeolicus* (PBP1a (*25*)).

Both sequence and structure alignments (*21*, *26*) between λ lysozyme and enzymes belonging to different classes of the lysozyme superfamily have indicated that λ lysozyme exhibits a hybrid character between c- and v-type lysozymes. The best structural alignments with hen and T4 lysozymes (ca. 60 C_α atoms with a rms distance close to 2 Å (*21*)) comprise the helix preceding the catalytic Glu (Glu19 in λ lysozyme), some β-strand segments, and the helix joining the two domains. A comprehensive discussion of the structural comparison of λ lysozyme with c- and v-type lysozymes can be found in Evrard et al. (*21*).

An interesting difference between hen and λ lysozymes is the lack of disulfide bonds in the latter. Hen lysozyme contains four disulfide bonds, and most refolding experiments have been carried out with these bonds intact. Indeed, refolding from the fully reduced form of the protein produces large quantities of aggregated species (*27*, *28*). Therefore, the presence of the native disulfide bridges at the initiation of the refolding process represents a situation that is distinct from that of the folding process *in vivo* (*29*, *30*). In this work, we have used a combination of biophysical techniques, including quenched-flow hydrogen exchange labeling monitored by 2D NMR and mass spectrometry, and stopped-flow fluorescence and CD spectroscopy, to investigate the refolding kinetics of λ lysozyme, which naturally lacks disulfide bridges.

MATERIALS AND METHODS

Enzymes and Chemicals. Ultrapure guanidinium chloride (GdmHCl) was obtained from Sigma Chemical Co. All other chemicals were of reagent grade.

Both λ lysozyme and the uniformly ^{15}N isotopically enriched enzyme were produced and purified as described (*31*). Lysozyme concentration was determined by both absorbance measurements at 280 nm (ε_M = 29450 $M^{-1}\cdot cm^{-1}$, calculated according to Pace et al. (*32*)) and the bicinchoninic acid protein assay reagent (Pierce).

Denaturant-Induced Unfolding Transitions. Equilibrium unfolding was studied at 25 °C in sodium acetate buffer, pH 5.6. Samples at various GdmHCl concentrations (0−3.5 M) were left to equilibrate for at least 12 h ($t_{1/2}$ unfolding <4 s). Unfolding curves were determined as described (*33*) by monitoring the changes in intrinsic fluorescence emission (λ_{ex} = 280 nm and λ_{em} = 341 nm) and CD at 222 nm, at 25 °C. The pH was checked to ensure a constant value throughout the whole transition, and the denaturant concentration was determined from refractive index measurements (*34*) using a R5000 hand refractometer from Atago. A protein concentration of ca. 0.2 mg/mL (~11 μM) was used for both fluorescence and CD measurements.

Kinetics of Unfolding and Refolding. All experiments were performed at 20 °C in 20 mM sodium acetate buffer, pH 5.6, using a protein concentration of 0.1 $mg\cdot mL^{-1}$ (5.6 μM). In all single mixing experiments, refolding reactions were initiated by a 10-fold dilution of lysozyme (1 $mg\cdot mL^{-1}$) unfolded in 3 M GdmHCl (note that under these conditions λ lysozyme unfolds with $\tau \sim 280$ ms), with refolding buffer containing denaturant

concentrations ranging from 0 to 1.2 M, yielding final concentrations in the 0.13−1.1 M range. Conversely, unfolding reactions were initiated by a 10-fold dilution of native lysozyme with the same buffer containing various amounts of GdmHCl to yield final concentrations ranging from 1.3 to 2 M.

Stopped-Flow Experiments. All kinetic experiments were performed using a Bio-Logic (Claix, France) SFM-400 stopped-flow device, coupled with a MOS-450/AF-CD spectrophotometer. Cells of 0.8 mm (FC-08) and 2 mm (FC-20) path lengths were used for fluorescence and CD measurements, respectively, and the dead time of the apparatus was found to be ~3 ms under all experimental conditions. This value was estimated by monitoring the fluorescence quenching reaction of *N*-acetyltryptophanamide by *N*-bromosuccinimide, as described in a technical note (no. 53) provided by the manufacturer (Bio-Logic, Claix, France).

For CD measurements, refolding kinetics were followed at 225 nm, whereas in intrinsic fluorescence experiments, an excitation wavelength of 280 nm was used, and total emission above 320 nm was monitored using a high-pass filter. Binding of the fluorescent dye ANS was estimated by recording total fluorescence emission above 450 nm, with an excitation wavelength of 350 nm. ANS (150 μM) was included in the refolding buffer, leading to final ANS and protein (P) concentrations of 15 and 5.6 μM, respectively (i.e., [ANS]/[P] = 2.7).

In double-mixing experiments, the protein (2 mg·mL^{-1}) was first unfolded for 2.5 s by a 2-fold dilution in 6 M GdmHCl and 20 mM sodium acetate buffer, pH 5.6 ($t_{1/2}$ unfolding < 0.2 s), and then immediately refolded by a 10-fold dilution in the refolding buffer. Final protein and GdmHCl concentrations were 0.1 mg·mL^{-1} and 0.3 M, respectively.

In single-mixing experiments, 7500 data points were sampled over the time course of one experiment, while 5000 points were acquired in double-mixing procedures.

Amide Hydrogen Exchange NMR Experiments in Native λ Lysozyme at pH 5.6 and 4.4. ^{1}H/^{2}H exchange rates were measured using 2 mM ^{15}N-labeled enzyme, on the basis of published resonance assignments (*31*). Exchange was initiated by a 10-fold dilution of a 2 mM ^{15}N-labeled protein sample in 10 mM HEPES, pH 7, into a ^2H_2O solution at pH 5.6 or 4.4. Samples were subsequently concentrated 10-fold by ultrafiltration at 4 °C to give a final protein concentration of 2 mM; this procedure was repeated five times (ca. 3 h in total) using a Vivaspin 4 ultrafiltration device (5000 MWCO PES; Sartorius, Goettingen, Germany). Following exchange and concentration, the protein sample was subsequently analyzed by 2D NMR, immediately or after time intervals ranging from 1 to 74 days. The sample was kept at 20 °C after each spectrum was taken.

NMR spectra were collected using a home-built 750 MHz NMR spectrometer, controlled with GE/Omega software and equipped with an Oxford Instruments Co. magnet and a home-built triple-resonance pulsed-field-gradient probe head. Sweep widths of 10526.3 and 2272.7 Hz in F_2 (^{1}H) and F_1 (^{15}N), respectively, were used for 2D ^{1}H−^{15}N HSQC spectra. A total of 128 complex ^{15}N increments of 16 scans were collected with 1024 complex points in the acquisition dimension. All experiments were collected at 20 °C. HSQC spectra were collected immediately after the final sample concentration step and 1, 2, 7, 18, 32, 50, and 74 days following the first spectrum. Exchange rates for more rapidly exchanging amides were determined from a series of 10 HSQC spectra collected at pH 4.4 over a period of ~40 h.

^{1}H/^{2}H exchange rates (k_{ex}) were determined from single exponential fits of peak heights, in the processed HSQC spectra, as a function of time. Protection factors were determined as described (*35*).

Hydrogen Exchange Pulse-Labeling Experiments. A deuterated guanidinium chloride solution (Gdm^{2}HCl) was prepared by three consecutive cycles of dissolution in ^2H_2O (99%; Cambridge Isotope Laboratories, Inc.) followed by freeze-drying. Samples were prepared using a Bio-Logic QFM-5 rapid-mixing quenched-flow device. In these experiments, a standard pulse-labeling procedure was performed, as described for hen lysozyme (*13*), in which deuterated unfolded λ lysozyme (5 mg·mL^{-1} in 3 M Gdm^{2}HCl and 500 mM DTT) was exposed to a high pH labeling pulse after various refolding periods (3.5−2000 ms) at 20 °C in 20 mM sodium acetate buffer, pH 5.6. The pH of the labeling pulse (pH 9.5) was adjusted to ensure that, at 20 °C, the length of the pulse (8.4 ms) corresponded to about 10 times the half-life ($t_{1/2}$) of the intrinsic ^{1}H/^{2}H exchange process; this calculation is based on data for hydrogen exchange rates in unstructured peptides, taking into account the activation energy for base catalysis of hydrogen exchange (*35*). Finally, ^{1}H/^{2}H exchange was quenched and refolding completed at pH 4.4 by dilution into 0.5 M acetic acid. Following pulse labeling, buffer exchange was carried out by exhaustive dilution and reconcentration of the samples at 4 °C, using a Vivaspin 4 ultrafiltration device, with 50 mM ammonium acetate, pH 4.5, for analysis by electrospray ionization mass spectrometry (ESI-MS) and with 10 mM deuterated sodium acetate, pH 4.5, for analysis by 2D NMR spectroscopy. Final protein concentrations of ~0.4 and ~10 mg·mL^{-1} (i.e., 22 and 560 μM) were reached for the ESI-MS and NMR samples, respectively. Samples were stored at 4 °C prior to analysis.

ESI-MS Analysis of Pulse-Labeling Samples. Experiments were performed with a 9.4 T Apex-Qe FTICR mass spectrometer (Bruker Daltonics, Billerica, MA). The lysozyme samples (~25 μM in 50 mM ammonium acetate, pH 4.5) were injected via an external Apollo electrospray ion source, at a flow rate of 2 μL/min, with the assistance of N_2 nebulizing gas. The off axis sprayer was grounded, the end plate was set to −3.5 kV, and the inlet capillary was set to −4 kV for the generation of lysozyme cations. N_2 heated drying gas (250 °C) was applied to assist desolvatation of ESI droplets. Ions were accumulated in the first hexapole for 3 s and transferred nonmass selectively through the quadrupole into the second hexapole for 10 ms. They were trapped for 10 ms in this second hexapole (h2) and then transferred through high-voltage ion optics and captured by static trapping in an ICR cell. All mass spectra were acquired with XMASS (version 7.0.8; Bruker Daltonics) in broad band mode from m/z 1600 to m/z 2400 with 512K data points and summed over 40 scans. A mass list, in which m/z values and peak heights are recorded, was created by DataAnalysis (version 3.4; Bruker Daltonics). Minimal smoothing of the raw data and baseline subtraction were performed in order to remove background noise. The peaks of interest were centroided with suitable parameters in order to obtain a vertical line passing through the center of gravity of each isotopic distribution. The centroid top (80%) and the experimental resolution (100000) were the same for all isotopic distributions, whereas the number of channels was optimized for each isotopic distribution. The resulting centered spectra give the center of the isotopic distributions and their "areas". These latter correspond to the sum of the intensities of the points across the peaks in the continuum trace,

and they were used to calculate the relative abundances of each species. All spectra shown are the +9 charge state expressed on a mass scale, but the scan range included other charge states to confirm that the reported features are independent of charge state. Each mass spectrum was obtained at least in duplicate, and samples were prepared a minimum of three times.

NMR Analysis of Pulse-Labeling Samples. 2D $^{1}H-^{15}N$ HSQC spectra of the pulse-labeled samples were collected as described above for native state exchange, except that 24 scans were collected per increment. Peak heights were determined using in-house software. A ^{1}H 1D NMR spectrum was collected for each pulse-labeled sample prior to collection of the 2D HSQC spectrum. The HSQC peak heights were normalized using the intensities of well-resolved upfield-shifted resonances in the 1D spectra; this corrected for the variation in protein concentration in the different samples.

Kinetic Analysis. Each kinetic trace resulted from the accumulation of approximately ten and five experiments for CD and fluorescence measurements, respectively. The resulting multiple data sets were fitted separately. These traces were analyzed according to a single exponential term (eq 1) or to the sum of two exponential terms (eq 2).

$$y_t = y_\infty + A \exp(-kt) \quad (1)$$

$$y_t = y_\infty + A_1 \exp(-k_1 t) + A_2 \exp(-k_2 t) \quad (2)$$

The rate constants were obtained by averaging over the data sets, and errors are calculated as standard deviations throughout.

The dependence of unfolding and folding rate constants on denaturant concentration was analyzed according to the linear relationship (*36*−*39*):

$$\ln(k_{obs}) = \ln\{k_f^{H_2O} \exp(-m_{kf}/RT[\text{denaturant}]) + k_u^{H_2O} \exp(m_{ku}/RT[\text{denaturant}])\} \quad (3)$$

where k_{obs} is the rate of unfolding or refolding measured at various GdmHCl concentrations, $k_f^{H_2O}$ and $k_u^{H_2O}$ are the values for folding and unfolding, respectively, in the absence of denaturant, and m_{kf}/RT and m_{ku}/RT are proportionality constants which describe the denaturant dependence.

The programs Grafit 5.0.10 (Erithacus Software Ltd.) and BioKine 32 V4.45 (Bio-Logic) were used for nonlinear least-squares analysis of the data.

RESULTS

Denaturant-Induced Unfolding Transitions. The stability of λ lysozyme at pH 5.6 was derived from GdmHCl-induced denaturation of the enzyme (Figure 2). Unfolding was found to be fully reversible, and the coincidence of the transition curves obtained by intrinsic fluorescence emission and far-UV CD measurements indicated that secondary and tertiary structure was destabilized concomitantly. These results suggest that λ lysozyme unfolds cooperatively in a single two-state transition (N ⇋ U), where only the native and unfolded states are significantly populated. Therefore, values of the thermodynamic parameters for the transition were computed assuming a two-state model: $\Delta G°_{N-U} = 25 \pm 2$ kJ·mol^{-1}, $m_{N-U} = 24 \pm 2$ kJ·mol^{-1}·M^{-1}, and $C_m = 1 \pm 0.2$ M. Note that an identical $\Delta G°$ value was found at pH 7, both with GdmHCl and urea (L. Banwarth, A. Di Paolo, and A. Matagne, unpublished results).

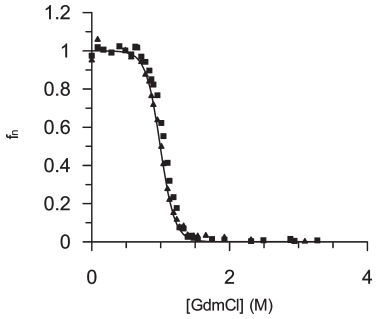

FIGURE 2: GdmHCl-induced equilibrium unfolding transition of λ lysozyme at pH 5.6, 20 °C, monitored by the change in fluorescence intensity at 341 nm (squares) and the change in ellipticity at 222 nm (triangles). Data were analyzed on the basis of a two-state model (*33*), and the solid line was drawn using the parameters obtained in the equilibrium denaturant-induced unfolding experiments ($\Delta G°_{N-U} = 25 \pm 2$ kJ·mol^{-1}, $m_{N-U} = 24 \pm 2$ kJ·mol^{-1}·M^{-1}, and $C_m = 1 \pm 0.2$ M). Data are presented as the fractional change in signal, f_n (*33*), as a function of GdmHCl concentration.

Stopped-Flow Optical Refolding Measurements. The refolding kinetics of λ lysozyme at a final GdmHCl concentration of 0.3 M, monitored by far-UV CD and by ANS fluorescence at 20 °C, gave very similar results (Figure 3A,C). After a burst phase, which was completed within the dead time of mixing (ca. 3 ms), two visible kinetic phases, with time constant values ($\tau = 1/k$) of 0.130 ± 0.014 s and 5 ± 1 s and relative amplitudes of $88 \pm 3\%$ and $12 \pm 2\%$ for the fast and slow phases, respectively, were observed. In contrast, measurement of intrinsic fluorescence (Figure 3B) during λ lysozyme refolding showed no dead-time change. Two phases were observed, however, with both time constant and relative amplitude values in agreement with those obtained by CD and ANS measurements. These experiments reveal that a transient kinetic intermediate accumulates in the dead time of the stopped-flow equipment, with $\tau < 1$ ms. It shows a substantial amount of secondary structure, as indicated by the presence of ~65% of the helical CD at 225 nm, but it lacks fixed tertiary organization as indicated by the absence of recovery of the native fluorescence. These properties, together with the capacity to induce enhancement of ANS fluorescence, which is maximal in the first few milliseconds of the reaction, are typical of molten globule intermediates, which have been found to be significantly populated early in the refolding kinetics of many proteins (*10*, *40*−*45*). The good agreement between the time constant values measured by the three methods (Table 1) indicates that they all monitor the same cooperative transitions. Note that the fluorescence refolding kinetics could be fitted equally well with three exponential phases, but with no statistically significant improvement of the fit (based on *F*-tests, not shown). The present interpretation was preferred on the basis of the good agreement of the calculated rate constants with those obtained by monitoring CD and ANS binding.

Double-Mixing Experiment. Since λ lysozyme contains five proline residues (all *trans*), it is possible that the slow phase ($\tau \approx 5$ s) results from *cis*/*trans* isomerization of non-native prolyl peptide bonds in the unfolded state. To test this hypothesis, a classical double-mixing experiment (*46*) was performed. In this experiment, the protein is fully unfolded for a period of time (2.5 s) that is too short to allow significant isomerization of proline-containing peptide bonds (time constant value of 300 s for the *trans* to *cis* isomerization at 25 °C is given by ref *47*) and then allowed to refold. Under such conditions, the intrinsic fluorescence of the native λ lysozyme molecules was recovered

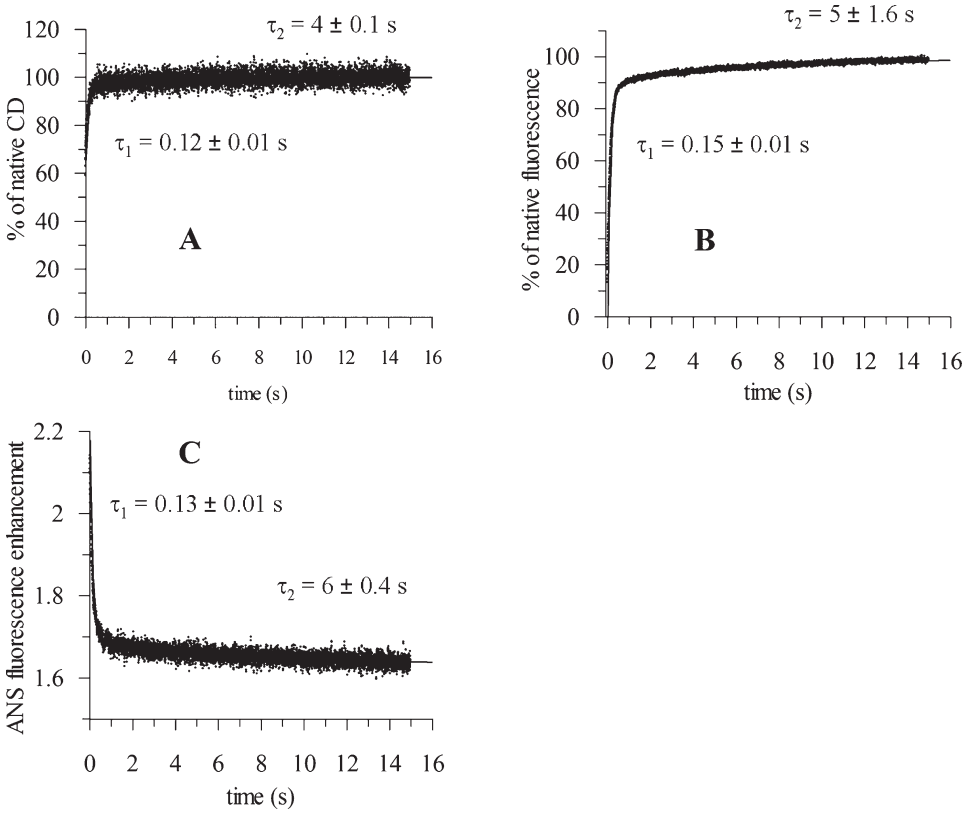

FIGURE 3: Refolding kinetics of λ lysozyme in 0.3 M GdmHCl, 20 mM sodium acetate, pH 5.6 and 20 °C, followed by (A) CD at 225 nm, (B) total intrinsic fluorescence emission above 320 nm, and (C) total ANS fluorescence emission above 450 nm. Double exponential functions (eq 2) have been fitted to the data. CD (A) and intrinsic fluorescence data (B) have been normalized to the total signal difference between the native (100%) and unfolded (0%) proteins under refolding conditions, whereas extrinsic fluorescence intensities in ANS binding kinetics (C) are expressed relative to the fluorescence of ANS in the presence of the unfolded protein in 3 M GdmHCl. The resulting average time constants are indicated. The dead time changes observed in (A) and (C) correspond to ~65% of the total signal recovery and ~2.2-fold signal enhancement, respectively.

Table 1: Kinetic Parameters (Time Constant (τ) and Amplitude (A)) for Refolding of λ Lysozyme after Rapid Mixing in 0.3 M GdmHCl, at pH 5.6, 20 °C[a]

experiment	A_1 (%)	τ_1 (s)	A_2 (%)	τ_2 (s)
intrinsic fluorescence	84 ± 3	0.147 ± 0.012	13 ± 5	5 ± 1.6
far-UV CD (225 nm)[b]	36 ± 4	0.120 ± 0.010	4 ± 0.1	4 ± 0.1
ANS fluorescence[b]	88 ± 12	0.130 ± 0.010	12 ± 2	6 ± 0.4
double mixing[b]	100	0.165 ± 0.022	nd	nd
$^1H/^2H$ exchange + NMR	70 ± 10	0.180 ± 0.040	nd	nd
$^1H/^2H$ exchange + ESI-MS	87 ± 3	0.150 ± 0.050	nd	nd

[a]Amplitudes are given as relative values of the two visible phases; nd, not detected. [b]These experiments showed a very rapid change of the measured signal, within the dead time of the experiment (i.e., hidden amplitude).

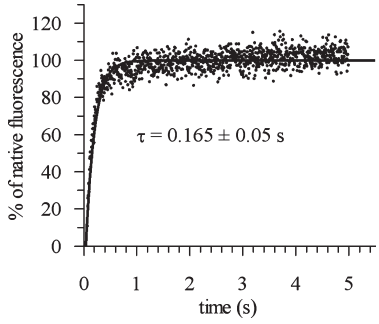

FIGURE 4: Refolding kinetics of λ lysozyme at 20 °C, after 2.5 s unfolding, monitored by the change in intrinsic fluorescence. In a stopped-flow double mixing experiment, the protein was unfolded in 3 M GdmHCl and then rapidly refolded by a 10-fold dilution to 0.3 M GdmHCl in 20 mM sodium acetate, pH 5.6. A single exponential function has been fitted to the data, normalized as described in the legend of Figure 3. *F*-test analysis indicated that the use of a double exponential function does not provide a statistically significant improvement to the fit. Note that data points were averaged to obtain 1000 points and hence increase the signal-to-noise ratio, as suggested by an anonymous reviewer.

on a much shorter time scale (Figure 4), with a time constant value (0.165 ± 0.020 s) characteristic of the fast folding phase. This observation indicates that the slow phase is probably associated with proline isomerization. Hence, the two phases observed in the refolding kinetics result from a heterogeneous population in the unfolded state, due to isomerization of prolyl peptide bonds. The slow phase, i.e., 12% of the amplitude measured by optical methods (Figure 2), corresponds to the folding of a fraction of unfolded protein containing proline peptide bond(s) in a non-native *cis* conformation.

Refolding and Unfolding Kinetics (*Chevron Plot*). A plot (known as a chevron plot (*37*)) of the logarithm of the rate constant for both folding and unfolding against the denaturant concentration is shown in Figure 5. Unfolding at high concentrations of denaturant shows a single exponential kinetic phase. Interestingly, the rate of the slow phase observed in the refolding kinetics shown in Figure 3 ($\tau \approx 5$ s) did not vary significantly with GdmHCl concentration, an observation further supporting the conclusion that this slow folding event corresponds to *cis*/*trans* isomerization of prolyl peptide bonds (*48*, *49*). At concentrations of denaturant ranging from 0.35 to 2 M (i.e., in the transition region between the native and the unfolded states; see Figure 2), the unfolding and non-proline-related refolding branches of the plot were found to be

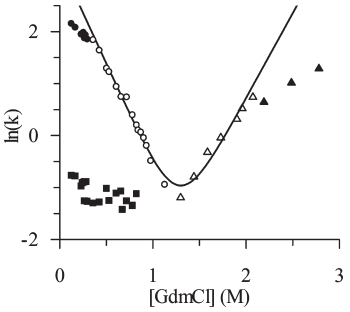

FIGURE 5: GdmHCl concentration dependence of the rate constants for λ lysozyme folding at pH 5.6, 20 °C. Circles and squares represent the observed rate constants (in s^{-1}) for fast and slow refolding, respectively, whereas triangles corresponds to the unfolding rate constants. The solid line represents the fit of eq 3 to the data obtained in the transition region (open symbols), using $k_f^{H_2O} = 28 \pm 4\ s^{-1}$, $k_u^{H_2O} = 0.0030 \pm 0.0016\ s^{-1}$, $m_{kf} = 9.5 \pm 0.4\ kJ \cdot mol^{-1} \cdot M^{-1}$, and $m_{ku} = 8 \pm 0.8\ kJ \cdot mol^{-1} \cdot M^{-1}$.

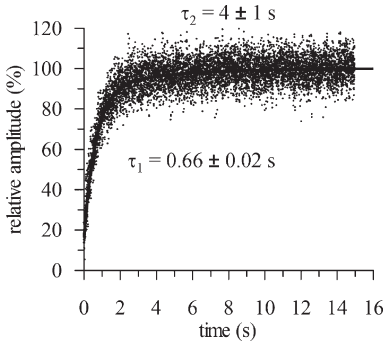

FIGURE 6: Refolding kinetics of λ lysozyme in 0.6 M GdmHCl at pH 5.6 and 20 °C, followed by CD at 225 nm. Normalization of the data is as in Figure 3, and a double exponential function has been fitted to the data. Relative amplitudes are 15%, 73%, and 12% for the burst, fast, and slow phases, respectively.

close to linear. Thus, in this concentration range eq 3 was used to fit the data, yielding values of the kinetic parameters given in the legend to Figure 5.

Considering that slow refolding of ca. 12% of molecules is due to *cis*/*trans* isomerization of prolyl peptide bonds, the equilibrium free energy for unfolding can be calculated as follows (*36*):

$$\Delta G^\circ_{kin} = RT\ \ln[(k_f^{H_2O}/k_u^{H_2O})(1/(1+K_{iso}))] \qquad (4)$$

where K_{iso} (= $[U_{slow}]/[U_{fast}]$) is a term accounting for the fraction of slow folding molecules, with *cis* proline isomers in the unfolded state. Stopped-flow optical experiments indicated that the relative amplitudes of the fast and slow phases are 88% and 12%, respectively, and thus $K_{iso} = 0.137$. Using the values of $k_f^{H_2O}$ and $k_u^{H_2O}$ calculated in Figure 5, a ΔG°_{kin} of 22 ± 2 $kJ \cdot mol^{-1}$ is obtained, which is identical within the error limit to the value (25 ± 2 $kJ \cdot mol^{-1}$) obtained under equilibrium conditions. Similarly, m_{kin} and C_m calculated from the kinetic data ($m_{kin} = m_{kf} + m_{ku}$) gives values of 17.5 ± 1 $kJ \cdot mol^{-1} \cdot M^{-1}$ and 1.25 ± 0.2 M, respectively. All of these values are in reasonable agreement with those obtained from equilibrium experiments and are thus consistent with λ lysozyme folding according to a two-state model in the transition region. Despite uncertainty in the kinetic *m* values, a Tanford β value ($\beta_T = m_{ku}/m_{N-U} = 1 - m_{kf}/m_{N-U}$ (*37*)) of 0.3−0.6 can be calculated. This suggests that, in comparison with other proteins folding with two-state kinetics (*37*), a rather low percentage (i.e., 30−60%) of the surface area of the enzyme is buried in the transition state for folding.

In contrast, outside the transition zone there is a clear downward curvature ("rollover") in the chevron plot, for both folding and unfolding of the enzyme. We observed that the refolding kinetics were independent of the protein concentration in the range from 0.01 to 0.2 $mg \cdot mL^{-1}$ (i.e., 0.6−11 μM), thus excluding the possibility that the downward curvature in the folding branch of the chevron plot is the result of aggregation (*50*). Rather, the deviation of the observed refolding kinetics from those expected for a two-state mechanism is most probably due to the kinetic molten globule intermediate, which is seen to accumulate during the dead time of the stopped-flow experiments. Significant population of this partially folded species at low denaturant concentrations is responsible for the deceleration in the refolding rate and gives rise to a rollover in the chevron plot. Interestingly, refolding of λ lysozyme monitored by far-UV CD measurements at 0.6 M GdmHCl (Figure 6) indicated that the amplitude (∼15%) of the burst phase is a lot weaker than at 0.3 M GdmHCl (Figure 3), suggesting that in the transition region the intermediate is highly destabilized and has only minor influence on the refolding rate. Above the C_m value (i.e., [GdmHCl] > 1.2 M), no evidence was found for the presence of unfolding intermediates, since full amplitude change is observed in all unfolding experiments. At these high denaturant concentrations, the nonlinear dependence of ln k_u against GdmHCl concentration might be associated with movement of the transition state structure closer to the native state (*51*, *52*).

Hydrogen Exchange of Native λ Lysozyme at pH 5.6 and 4.4. The rates of $^1H/^2H$ exchange (k_{ex}) of 49 amide protons of native λ lysozyme were measured at pH 5.6 and 20 °C by recording 2D $^1H-^{15}N$ HSQC spectra at various time intervals. Exchange of an additional set of 17 amide NHs was also observed at this pH but was too fast to be measured. This could be achieved, however, by lowering the pH to 4.4. Exchange of the remaining 86 (^{15}N assignments for the N-terminal residue, Met1, and for the five proline residues have not been obtained (*31*)) amide hydrogens was much too fast to be measured in these experiments. Rates of exchange are dependent on the protein structure, and this is generally expressed in terms of protection factors, defined as $P = k_{ex}/k_{int}$, where k_{int} is the intrinsic exchange rate for each amide hydrogen atom in unstructured peptides under the same conditions, taking into account effects of the solution pH, the temperature, and the local amino acid sequence on amide exchange (*35*).

The protection factors determined for the native enzyme are given in Figure 7, as a function of the protein sequence. A total of 66 amide protons (i.e., ∼43% of all amide NHs) were found to be protected, with *P* values falling between 16 and 3.3×10^6. Protected amides occur in both domains, mainly in the α-helices and β-strands, indicating that the various elements of secondary structure (ca. 51% of the complete amino acid sequence) afford significant protection against exchange under native conditions. Thus, the site-specific observation of the time-course of protection from exchange of these amide protons by NMR ($^1H-^{15}N$ HSQC experiment), as structure is formed during folding, will allow the formation of the different structural elements of the protein during the course of refolding to be monitored. Close examination of the data in Figure 7 indicates, however, that no protection against exchange is found in strands β3 and β4. This observation is in good agreement with the conclusion (*21*, *22*) that this region of the enzyme structure is highly mobile.

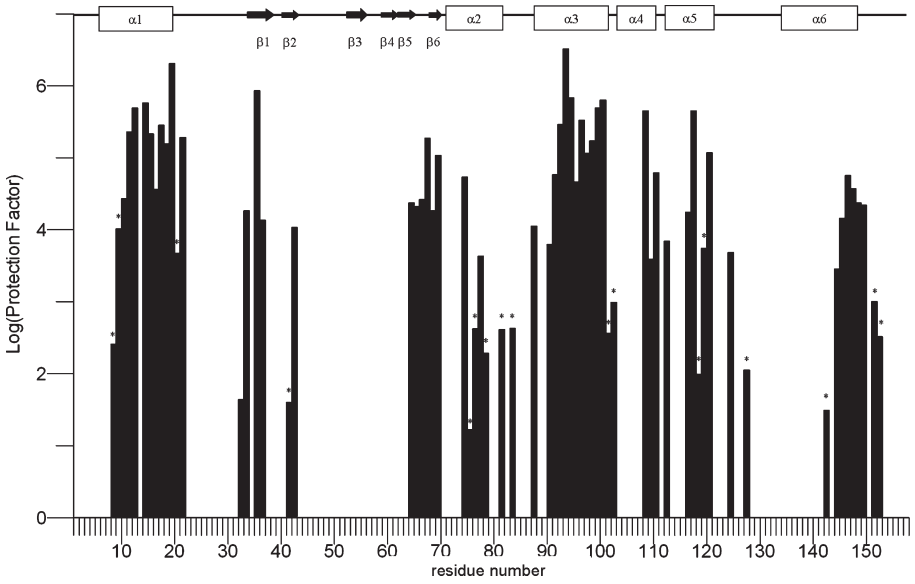

FIGURE 7: Amide hydrogen exchange in native λ lysozyme. The histogram shows the distribution of protection factors for the native enzyme at pH 5.6 and 20 °C versus amino acid residue number. Exchange rates for more rapidly exchanging amides (indicated by *) were determined at pH 4.4. Note that the peaks for residues 13 and 143, 34 and 61, and 111 and 150 overlap in the HSQC spectrum and thus could not be distinguished. Regions of secondary structure are indicated schematically.

Pulsed $^1H/^2H$ Exchange Labeling Measured by 2D NMR. Refolding of λ lysozyme was initiated by an 11-fold dilution into the refolding buffer, and hydrogen exchange pulse labeling was carried out as described in Materials and Methods. The time scale (0.0035−2 s) for these experiments was chosen to correspond to that of the rapid ($\tau \approx 0.13$ s) phase of refolding seen by optical method and does not cover entirely the slow phase ($\tau \approx 5$ s) because at pH 5.6 the half-life of amide hydrogen exchange is about 16 s (*53*) . The structural details of the folding reaction were obtained by analyzing the samples by 2D $^1H-^{15}N$ HSQC measurements. Figure 8 displays the protection time courses obtained for individual amides, grouped according to their distribution in the native secondary structure elements. A total of 54 amide NHs, out of the 66 found to be protected in the native protein (Figure 7), could be monitored in this way; these belong mostly to well-organized elements of structure (i.e., sheets and helices). In addition, amides from ten residues located in loop structures (see Table 2 in Supporting Information) could also be monitored. In comparison with native state exchange experiments, 12 amides could not be observed in the refolding kinetics. This is due either to very high exchange rates under the experimental conditions (i.e., residues 32, 75, 76, 127, and 142, which protection factors were all determined at pH 4.4) or to the low quality of the kinetic data (i.e., residues 36, 65, 66, 77, 94, 99, and 124).

All of the kinetics were found to be monophasic, and a single exponential function could be used to fit the data satisfactorily (Figure 8). The resulting curves are all virtually identical, with average time constant and amplitude values of 0.180 ± 0.040 s and 0.70 ± 0.10, respectively (see Table 2 in Supporting Information). The results indicate that all detectable amides acquire protection from exchange coincidentally, with simple monoexponential time courses. No intermediate partially protected species are observed in these experiments, and folding appears to be highly cooperative. That no significant protection from $^1H/^2H$ exchange is observed after 3.5 ms of folding suggests that the secondary structure elements formed early in the kinetic intermediate observed in stopped-flow optical experiments are not sufficiently stable to afford protection under our experimental conditions. This is consistent with the properties of the low pH molten globules of bovine, guinea pig, and human α-lactalbumin (*54*−*57*), for which protection factor values substantially lower than those observed in the native state (i.e., 100−500 vs ∼10^7) were reported.

Pulse-labeling $^1H/^2H$ exchange experiments reveal that ca. 30% of molecules are not protected from exchange even after 2 s. This can be attributed, at least in part, to the minority of molecules (∼12%) that refold on a longer time scale ($\tau \approx 5$ s), presumably as a consequence of slow *cis* → *trans* isomerization of non-native proline isomers. Calculation of biexponential curves (not shown), using time constant and amplitude values from $^1H/^2H$ exchange kinetics and stopped-flow optical experiments for the fast ($\tau \approx 0.18$ s) and slow phases ($\tau \approx 5$ s), respectively, indicated that this hypothesis is consistent with the data in Figure 8. Similarly, isomerization of prolyl peptide bonds was taken as responsible for incomplete protection in around 17% of hen lysozyme molecules after 2 s of refolding (*12*, *13*, *18*). In our $^1H/^2H$ exchange experiments, the existence of ∼12% of slow refolding molecules due to *cis*/*trans* isomerization of Xaa−Pro peptide bonds is not sufficient, however, to explain the ca. 30% of unprotected molecules. We suspect that some back-exchange of ^2H for ^1H occurred following quenching and prior to the final buffer exchange into the ^2H_2O buffer; because of the large amount of protein required for NMR, preparation of the samples required several hours. This is most probably responsible for an additional ca. 15−20% lack of protection in these experiments (see below).

Pulsed $^1H/^2H$ Exchange Labeling Measured by ESI-MS. Further insights into the cooperativity of folding and on the population of intermediates can be obtained by detection of hydrogen exchange labeling by ESI-MS (*18*). Samples both identical to those used for the above NMR experiments and prepared independently under similar conditions were analyzed, and the results are illustrated in Figure 9A. Two well-defined populations were detected over the time course of the experiment. The lower mass species (17819 ± 1 Da, monoisotopic mass; $m/z \approx$ 1982 in Figure 9A) corresponds to the unprotected enzyme.

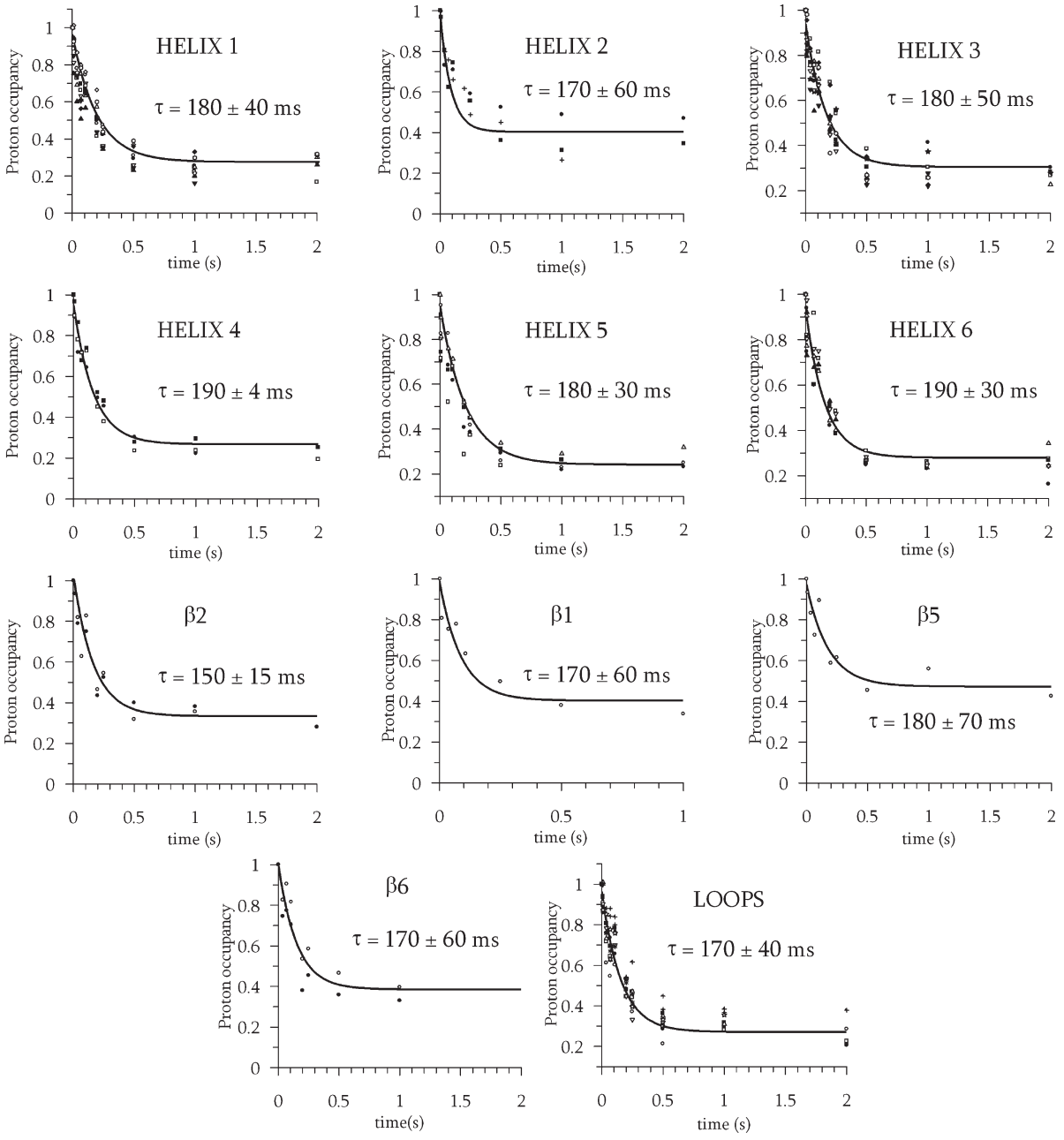

FIGURE 8: Time course for the amide protection from exchange during the refolding of λ lysozyme at pH 5.6 and 20 °C. The continuous lines were constructed from the analytical solutions for the time courses of individual amides in each native secondary structural element, using the parameters given in Table 2 (Supporting Information).

Its mass is slightly greater than that calculated for fully protonated λ lysozyme (17815 Da) and checked experimentally, by ESI-MS, as a control (data not shown). This minor difference is probably due to the presence of residual deuterons (~2%) in the labeling pulse, although the possible occurrence of early marginally protected intermediates cannot be ignored. The other peak, at 17862 ± 1 Da ($m/z \approx 1987$ in Figure 9A), protects 48 ± 2 sites significantly from exchange, in close agreement with the number of amides (54) observed in HSQC NMR experiments.

A single exponential function fits well to the kinetics of the disappearance of the lower mass species and the appearance of the higher mass species (Figure 9B), and the corresponding time constant values ($\tau = 0.15 \pm 0.05$ s) are identical. These results confirm the absence of any partially protected species and support the conclusion that folding is highly cooperative, with concomitant folding of the two structural domains.

Interestingly, in these experiments only ca. 15% of molecules were found unprotected from exchange after 2 s, which can be explained on the sole basis of the population (~12%) of slow refolding molecules. This is significantly less than observed in the samples analyzed by NMR. Although all $^1H/^2H$ exchange samples were prepared according to the same procedure, NMR samples were exposed to an H_2O buffer containing borate and GdmHCl for a significantly longer period of time prior to final buffer exchange. This is likely to explain the difference between the two sets of experiments and support the above conclusion that ca. 15−20% of the absence of protection in the NMR samples is due to back-exchange.

DISCUSSION

Chemical-induced unfolding of lysozyme from bacteriophage λ (Figure 2) showed a two-state transition between the native (N)

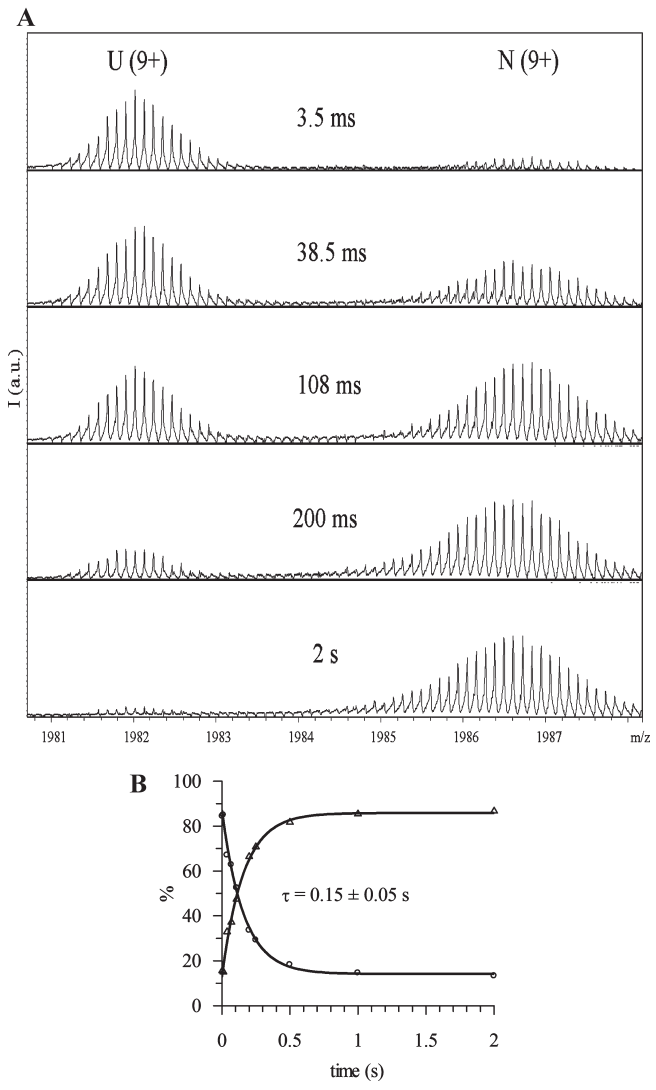

FIGURE 9: Refolding kinetics of λ lysozyme at 20 °C, as monitored by hydrogen exchange labeling and ESI-MS. (A) ESI mass spectra of the +9 charge state at different refolding times. Two well-defined populations are detected. They correspond to the unprotected protein (U), with a monoisotopic molecular mass of 17819 ± 1 Da, and the protected protein (N), with a monoisotopic molecular mass of 17862 ± 1 Da. (B) Time courses of the population of the unprotected state (circles) and species with native-like protection (triangles) are shown. The solid lines have been obtained by fitting single exponential functions to the data, with $\tau = 0.15$ s.

and the unfolded (U) states, without significant population of any intermediate structured species. The experimental *m* value (ca. 24 kJ·mol^{-1}·M^{-1}) is even higher than that calculated (16.3 kJ·mol^{-1}·M^{-1}) from the size of the protein (*58*), which is in favor of a fully cooperative unfolding mechanism, from which any deviation should in fact lower the *m* value (*58*, *59*). Based on a two-state model analysis, the Gibbs free energy of unfolding of λ lysozyme ($\Delta G°_{N-U}$) was calculated to be ca. 25 kJ·mol^{-1}, which is half the values estimated for both T4 and hen lysozyme (ca. 50 kJ·mol^{-1} (*60*, *61*)). In comparison with hen lysozyme, the significantly lower conformational stability of λ lysozyme cannot merely be explained on the basis of its lack of disulfide bridges (four in hen lysozyme), since T4 lysozyme is also devoid of such covalent links.

The X-ray structure (*21*) of λ lysozyme contains three molecules in the unit cell and reveals molecules in both open and closed conformations. Residues 51−60 and 128−141 (Figure 1), which form the so-called lower and upper lips of the catalytic pocket, are observed in significantly different environments in the two conformations. The distance between these lips is 23 and 10 Å in the open and closed conformations, respectively. The active site is located in a deep cleft between these two regions. A second X-ray structure (*22*), obtained with the inhibitor chitohexaose bound, shows the protein in the more closed conformation. We have monitored ^{1}H/^{2}H exchange in λ lysozyme by using HSQC spectra for the protein dissolved in ^2H_2O (Figure 7). Cross-peaks from 66 amides are observed, which arise mainly from residues located in both α-helix and β-sheet secondary structures. Thus, under native conditions exchange could be followed for ~43% of all amides, which is less than for both T4 (~71% (*4*)) and hen (~54% (*62*)) lysozymes. In addition, with the latter the most protected amide hydrogens were found to have protection factors around 10^8, i.e., approximately 2 orders of magnitude greater than for λ lysozyme (note that protection factors for T4 lysozyme were not reported). This might indicate a greater flexibility of λ lysozyme. Interestingly, no protection from ^{1}H/^{2}H exchange is observed for residues 52−61 in domain I, which are involved in a hydrogen-bonded antiparallel β-sheet in the open conformation but not in the closed one. In the other domain, protection is observed for the amides of residues 142 and 144−149, which are located in the C-terminal end of helix α6 (residues 135−149). No protection is observed, however, in the 135−141 region. X-ray diffraction studies (*21*) indicated that in the open conformation about one turn of helix α6 is lost. Our results support the hypothesis (*22*) that in solution and in the absence of bound substrate residues 51−60 and 128−141 are in highly mobile regions and can populate multiple conformations, one of them resembling the substrate bound (i.e., closed) conformation. ^{15}N relaxation measurements carried out in solution (A. Di Paolo, A. Matagne, and C. Redfield, unpublished results) indicated significant dynamics on the picosecond time scale for residues 52−61 and 129−140, suggesting that λ lysozyme interconverts rapidly between the open and closed conformations observed in the crystal. In the presence of substrate, X-ray data (*22*) suggested that the dynamics of these two highly flexible regions are dramatically reduced and that a single (closed) conformation is populated. Quite remarkably, a restriction in mobility (in regions 51−60 and 128−141) upon sugar binding is associated with a reduction in secondary structure content (β3−β4 and N-terminal end of α6, respectively). Altogether, these results suggest that λ lysozyme is a highly dynamic molecule and this remarkable flexibility is in good agreement with the relatively modest conformational stability of the enzyme. This is reminiscent of psychrophilic enzymes for which lower stability and greater flexibility, especially at or near the active site, have been established as a process of adaptation to cold (*63*). This deserves, however, further investigation.

A combination of complementary spectroscopic probes, including intrinsic and extrinsic (ANS-related) fluorescence and far-UV CD, were used to follow the kinetics of folding of this enzyme in 0.3 M GdmHCl, pH 5.6, 20 °C (Figure 3). Within the dead time (~3 ms) of the stopped-flow experiment, λ lysozyme acquires a substantial proportion (~65%) of its native ellipticity at 225 nm, and maximal ANS fluorescence occurs. No significant change in intrinsic fluorescence is observed, however, indicating no major changes in the exposure of aromatic residues to the solvent. Thus, at the end of the burst phase, secondary structure is formed in an intermediate, which exhibits substantial ANS binding. This is consistent with very fast ($\tau < 1$ ms) hydrophobic

collapse into a species with a large amount of fluctuating secondary structure. Such kinetic intermediates have been observed in many proteins, including T4 (*6*) and hen lysozymes (*10*). They display properties of molten globules observed under equilibrium conditions (*40*, *45*, *64*, *65*).

Following the very rapid formation of the kinetic molten globule, the three optical methods revealed two distinct kinetic phases (Figure 3), with relative amplitudes and time constants of 88% and 12% and 0.13 s and 5 s, respectively. When the protein was unfolded in 3 M GdmHCl for only 2.5 s and then refolded (in a double mixing experiment; Figure 4), the enzyme was fully renatured (in 0.3 M urea) within about 1 s. This suggests that the slow phase results from a heterogeneous population in the denatured state due to proline isomerization. This conclusion is further supported by the absence of an effect of the denaturant concentration on the time constant characteristic for this relatively slow event (Figure 4).

For the majority of refolding molecules, acquisition of native-like fluorescence and far-UV CD signals, and reduction in ANS fluorescence (i.e., binding) occur simultaneously on a millisecond time scale, with $\tau = 0.130 \pm 0.014$ s (Figure 3). These results suggest that refolding from the burst phase intermediate to the native state is a highly cooperative reaction, with no significant population of partially folded species. The effect of denaturant on unfolding and refolding kinetics (Figures 5 and 6) indicated that the intermediate is significantly destabilized at concentrations above 0.3 M. Analysis of the data in the form of a chevron plot showed apparent simple two-state folding ($U \rightleftharpoons N$) in the concentration range (0.35−2 M) corresponding to the equilibrium two-state transition. Calculation of the forward ($k_f^{H_2O}$) and reverse ($k_u^{H_2O}$) rate constants gave the same Gibbs free energy of unfolding (ca. 22 kJ·mol^{-1}) as that measured directly in equilibrium experiments. In addition, the sum of the forward and reverse *m* values (ca. 18 kJ·mol^{-1}·M^{-1}), although slightly lower, is also consistent with the *m* value for equilibrium unfolding.

Deviation from the simple V-shaped curve in the plot (Figure 5) of the logarithm of the rate constants for both folding and unfolding against the concentration of denaturant occurs, however, outside the transition zone. At low denaturant concentration, downward curvature is due to the accumulation of the burst phase intermediate, and λ lysozyme folding is thus apparently three-state under these experimental conditions. In contrast, the rollover observed in the chevron plot at high denaturant concentrations cannot be attributed to the presence of intermediate species on the unfolding pathway. In this case, a curved chevron plot is commonly explained by a movement of the transition state toward the native state upon destabilization (*66*).

Finally, quenched-flow hydrogen exchange labeling monitored by NMR and ESI-MS (Figures 8 and 9) indicated fast ($\tau = 0.180 \pm 0.040$ s) and simultaneous protection at about 50 amide sites throughout the secondary structure in a single major phase. Even amides located in more irregular structure were protected with similar kinetics. These experiments demonstrate that no intermediate species, other than the molten globule observed at the onset of the reaction in stopped-flow optical experiments, are populated during folding. The lack of protection from exchange observed after 3.5 ms of folding suggests that no stable native-like hydrogen bonds have formed yet and, hence, that the secondary structure elements observed by far-UV CD are still highly mobile. This is confirmed by stopped-flow intrinsic fluorescence measurements, which indicate that no stable tertiary contacts have formed on this time scale. Folding from this partially folded species to the native state appears to be a highly cooperative event, best described by a single two-state mechanism (i.e., $I \rightarrow N$ under conditions favoring the native state), where synchronous structure formation occurs in both domains in at least a substantial proportion (ca. 88%) of molecules. In that respect, the folding process of λ lysozyme differs markedly from that of hen lysozyme, for which the two structural domains that characterize the native structure of all lysozymes have been unambiguously shown to behave as independent structural units (*12*, *13*, *18*). Furthermore, with hen lysozyme kinetic partitioning between fast and slow refolding molecules occurs (*13*, *17*, *18*), which might result from conformational heterogeneity in the collapsed state (*20*) but not from residual interactions (*67*) or *cis* proline isomers (*68*) in the denatured state.

The four preexisting disulfide bonds in hen lysozyme might be one of the determinants for the reduced cooperativity and the heterogeneity of the folding process (*11*, *69*). However, although results obtained with λ lysozyme seem to support this hypothesis, no clear conclusion can be drawn concerning the role of preformed disulfide bridges in the folding of hen lysozyme. Despite a clear similarity in the organization of hen and λ lysozymes into two domains, the two enzymes display many structural differences. Interestingly, the existence of an intermediate with native-like structure in the two structural domains was demonstrated during folding of hen lysozyme, both with its four native disulfide bonds intact (*17*, *70*) or reduced (*28*). Folding to the fully native state is then achieved after final reorganization and docking of the two partially structured domains to form the active site. Although a similar folding step was not observed for T4 and λ lysozymes, its existence cannot be ruled out. This deserves further investigation.

ACKNOWLEDGMENT

The authors thank Jean-Marie Frère, Roger H. Pain, and Mireille Dumoulin for many enlightening discussions. We also acknowledge J.-M. Frère and Julie Vandenameele for critical reading of the manuscript.

SUPPORTING INFORMATION AVAILABLE

One table detailing the protection of amides during the refolding of λ lysozyme. This material is available free of charge via the Internet at http://pubs.acs.org.

REFERENCES

1. Vollmer, W., Joris, B., Charlier, P., and Foster, S. (2008) Bacterial peptidoglycan (murein) hydrolases. *FEMS Microbiol. Rev. 32*, 259–286.
2. Baase, W. A., Liu, L., Tronrud, D. E., and Matthews, B. W. (2010) Lessons from the lysozyme of phage T4. *Protein Sci. 19*, 631–641.
3. Elwell, M., and Schellman, J. (1975) Phage T4 lysozyme. Physical properties and reversible unfolding. *Biochim. Biophys. Acta 386*, 309–323.
4. Llinas, M., Gillespie, B., Dahlquist, F. W., and Marqusee, S. (1999) The energetics of T4 lysozyme reveal a hierarchy of conformations. *Nat. Struct. Biol. 6*, 1072–1078.
5. Chen, B. L., Baase, W. A., and Schellman, J. A. (1989) Low-temperature unfolding of a mutant of phage T4 lysozyme. 2. Kinetic investigations. *Biochemistry 28*, 691–699.
6. Lu, J., and Dahlquist, F. W. (1992) Detection and characterization of an early folding intermediate of T4 lysozyme using pulsed hydrogen exchange and two-dimensional NMR. *Biochemistry 31*, 4749–4756.
7. Cellitti, J., Bernstein, R., and Marqusee, S. (2007) Exploring subdomain cooperativity in T4 lysozyme II: uncovering the C-terminal subdomain as a hidden intermediate in the kinetic folding pathway. *Protein Sci. 16*, 852–862.

8. Kato, H., Vu, N. D., Feng, H., Zhou, Z., and Bai, Y. (2007) The folding pathway of T4 lysozyme: an on-pathway hidden folding intermediate. *J. Mol. Biol. 365*, 881–891.
9. Kato, H., Feng, H., and Bai, Y. (2007) The folding pathway of T4 lysozyme: the high-resolution structure and folding of a hidden intermediate. *J. Mol. Biol. 365*, 870–880.
10. Ikeguchi, M., Kuwajima, K., Mitani, M., and Sugai, S. (1986) Evidence for identity between the equilibrium unfolding intermediate and a transient folding intermediate: a comparative study of the folding reactions of alpha-lactalbumin and lysozyme. *Biochemistry 25*, 6965–6972.
11. Chaffotte, A. F., Guillou, Y., and Goldberg, M. E. (1992) Kinetic resolution of peptide bond and side chain far-UV circular dichroism during the folding of hen egg white lysozyme. *Biochemistry 31*, 9694–9702.
12. Miranker, A., Radford, S. E., Karplus, M., and Dobson, C. M. (1991) Demonstration by NMR of folding domains in lysozyme. *Nature 349*, 633–636.
13. Radford, S. E., Dobson, C. M., and Evans, P. A. (1992) The folding of hen lysozyme involves partially structured intermediates and multiple pathways. *Nature 358*, 302–307.
14. Gladwin, S. T., and Evans, P. A. (1996) Structure of very early protein folding intermediates: new insights through a variant of hydrogen exchange labelling. *Folding Des. 1*, 407–417.
15. Morgan, C. J., Miranker, A., and Dobson, C. M. (1998) Characterization of collapsed states in the early stages of the refolding of hen lysozyme. *Biochemistry 37*, 8473–8480.
16. Matagne, A., Jamin, M., Chung, E. W., Robinson, C. V., Radford, S. E., and Dobson, C. M. (2000) Thermal unfolding of an intermediate is associated with non-Arrhenius kinetics in the folding of hen lysozyme. *J. Mol. Biol. 297*, 193–210.
17. Matagne, A., Radford, S. E., and Dobson, C. M. (1997) Fast and slow tracks in lysozyme folding: insight into the role of domains in the folding process. *J. Mol. Biol. 267*, 1068–1074.
18. Miranker, A., Robinson, C. V., Radford, S. E., Aplin, R. T., and Dobson, C. M. (1993) Detection of transient protein folding populations by mass spectrometry. *Science 262*, 896–900.
19. Dobson, C. M., Evans, P. A., and Radford, S. E. (1994) Understanding how proteins fold: the lysozyme story so far. *Trends Biochem. Sci. 19*, 31–37.
20. Matagne, A., and Dobson, C. M. (1998) The folding process of hen lysozyme: a perspective from the "new view". *Cell. Mol. Life Sci. 54*, 363–371.
21. Evrard, C., Fastrez, J., and Declercq, J. P. (1998) Crystal structure of the lysozyme from bacteriophage lambda and its relationship with V and C-type lysozymes. *J. Mol. Biol. 276*, 151–164.
22. Leung, A. K., Duewel, H. S., Honek, J. F., and Berghuis, A. M. (2001) Crystal structure of the lytic transglycosylase from bacteriophage lambda in complex with hexa-N-acetylchitohexaose. *Biochemistry 40*, 5665–5673.
23. Taylor, A., Das, B. C., and van Heijenoort, J. (1975) Bacterial-cell-wall peptidoglycan fragments produced by phage A or Vi I1 endolysin and containing 1,6-anhydro-N-acetylmurarnic acid. *Eur. J. Biochem. 53*, 47–54.
24. Lovering, A. L., de Castro, L. H., Lim, D., and Strynadka, N. C. (2007) Structural insight into the transglycosylation step of bacterial cell-wall biosynthesis. *Science 315*, 1402–1405.
25. Yuan, Y., Barrett, D., Zhang, Y., Kahne, D., Sliz, P., and Walker, S. (2007) Crystal structure of a peptidoglycan glycosyltransferase suggests a model for processive glycan chain synthesis. *Proc. Natl. Acad. Sci. U.S.A. 104*, 5348–5353.
26. Jespers, L., Sonveaux, E., and Fastrez, J. (1992) Is the bacteriophage lambda lysozyme an evolutionary link or a hybrid between the C and V-type lysozymes? Homology analysis and detection of the catalytic amino acid residues. *J. Mol. Biol. 228*, 529–538.
27. Goldberg, M. E., Rudolph, R., and Jaenicke, R. (1991) A kinetic study of the competition between renaturation and aggregation during the refolding of denatured-reduced egg white lysozyme. *Biochemistry 30*, 2790–2797.
28. van den Berg, B., Chung, E. W., Robinson, C. V., and Dobson, C. M. (1999) Characterisation of the dominant oxidative folding intermediate of hen lysozyme. *J. Mol. Biol. 290*, 781–796.
29. Gething, M. J., and Sambrook, J. (1992) Protein folding in the cell. *Nature 355*, 33–45.
30. Hartl, F. U., and Hayer-Hartl, M. (2002) Molecular chaperones in the cytosol: from nascent chain to folded protein. *Science 295*, 1852–1858.
31. Di Paolo, A., Duval, V., Matagne, A., and Redfield, C. (2010) Backbone ^{1}H, ^{13}C, and ^{15}N resonance assignments for lysozyme from bacteriophage lambda. *Biomol. NMR Assign. 4*, 111–114.
32. Pace, C. N., Vajdos, F., Fee, L., Grimsley, G., and Gray, T. (1995) How to measure and predict the molar absorption coefficient of a protein. *Protein Sci. 4*, 2411–2423.
33. Vandenameele, J., Lejeune, A., Di Paolo, A., Brans, A., Frère, J.-M., Schmid, F. X., and Matagne, A. (2010) Folding of class A beta-lactamases is rate-limited by peptide bond isomerization and occurs via parallel pathways, *Biochemistry 49*, 4264−4275.
34. Nozaki, Y. (1972) The preparation of guanidine hydrochloride. *Methods Enzymol. 26* (Part C), 43–50.
35. Bai, Y., Milne, J. S., Mayne, L., and Englander, S. W. (1993) Primary structure effects on peptide group hydrogen exchange. *Proteins 17*, 75–86.
36. Jackson, S. E., and Fersht, A. R. (1991) Folding of chymotrypsin inhibitor 2. 1. Evidence for a two-state transition. *Biochemistry 30*, 10428–10435.
37. Fersht, A. R. (1998) Structure and Mechanism in Protein Science—A Guide to Enzyme Catalysis and Protein Folding, WH. Freeman and Co. New York.
38. Baldwin, R. L. (1996) On-pathway versus off-pathway folding intermediates. *Folding Des. 1*, R1–R8.
39. Khorasanizadeh, S., Peters, I. D., and Roder, H. (1996) Evidence for a three-state model of protein folding from kinetic analysis of ubiquitin variants with altered core residues. *Nat. Struct. Biol. 3*, 193–205.
40. Ptitsyn, O. B., Pain, R. H., Semisotnov, G. V., Zerovnik, E., and Razgulyaev, O. I. (1990) Evidence for a molten globule state as a general intermediate in protein folding. *FEBS Lett. 262*, 20–24.
41. Jennings, P. A., and Wright, P. E. (1993) Formation of a molten globule intermediate early in the kinetic folding pathway of apomyoglobin. *Science 262*, 892–896.
42. Balbach, J., Forge, V., van Nuland, N. A., Winder, S. L., Hore, P. J., and Dobson, C. M. (1995) Following protein folding in real time using NMR spectroscopy. *Nat. Struct. Biol. 2*, 865–870.
43. Udgaonkar, J. B., and Baldwin, R. L. (1995) Nature of the early folding intermediate of ribonuclease A. *Biochemistry 34*, 4088–4096.
44. Raschke, T. M., and Marqusee, S. (1997) The kinetic folding intermediate of ribonuclease H resembles the acid molten globule and partially unfolded molecules detected under native conditions. *Nat. Struct. Biol. 4*, 298–304.
45. Kuwajima, K. (1989) The molten globule state as a clue for understanding the folding and cooperativity of globular-protein structure. *Proteins 6*, 87–103.
46. Brandts, J. F., Halvorson, H. R., and Brennan, M. (1975) Consideration of the possibility that the slow step in protein denaturation reactions is due to cis-trans isomerism of proline residues. *Biochemistry 14*, 4953–4963.
47. Kiefhaber, T., Kohler, H. H., and Schmid, F. X. (1992) Kinetic coupling between protein folding and prolyl isomerization. I. Theoretical models. *J. Mol. Biol. 224*, 217–229.
48. Schmid, F. X., and Baldwin, R. L. (1979) The rate of interconversion between the two unfolded forms of ribonuclease A does not depend on guanidinium chloride concentration. *J. Mol. Biol. 133*, 285–287.
49. Jackson, S. E., and Fersht, A. R. (1991) Folding of chymotrypsin inhibitor 2. 2. Influence of proline isomerization on the folding kinetics and thermodynamic characterization of the transition state of folding. *Biochemistry 30*, 10436–10443.
50. Silow, M., and Oliveberg, M. (1997) Transient aggregates in protein folding are easily mistaken for folding intermediates. *Proc. Natl. Acad. Sci. U.S.A. 94*, 6084–6086.
51. Matouschek, A., and Fersht, A. R. (1993) Application of physical organic chemistry to engineered mutants of proteins: Hammond postulate behavior in the transition state of protein folding. *Proc. Natl. Acad. Sci. U.S.A. 90*, 7814–7818.
52. Otzen, D. E., Kristensen, O., Proctor, M., and Oliveberg, M. (1999) Structural changes in the transition state of protein folding: alternative interpretations of curved chevron plots. *Biochemistry 38*, 6499–6511.
53. Jeng, M. F., and Englander, S. W. (1991) Stable submolecular folding units in a non-compact form of cytochrome *c*. *J. Mol. Biol. 221*, 1045–1061.
54. Baum, J., Dobson, C. M., Evans, P. A., and Hanley, C. (1989) Characterization of a partly folded protein by NMR methods: studies on the molten globule state of guinea pig alpha-lactalbumin. *Biochemistry 28*, 7–13.
55. Chyan, C. L., Wormald, C., Dobson, C. M., Evans, P. A., and Baum, J. (1993) Structure and stability of the molten globule state of guinea-pig alpha-lactalbumin: a hydrogen exchange study. *Biochemistry 32*, 5681–5691.
56. Forge, V., Wijesinha, R. T., Balbach, J., Brew, K., Robinson, C. V., Redfield, C., and Dobson, C. M. (1999) Rapid collapse and slow

structural reorganisation during the refolding of bovine alpha-lactalbumin. *J. Mol. Biol. 288*, 673–688.
57. Schulman, B. A., Redfield, C., Peng, Z. Y., Dobson, C. M., and Kim, P. S. (1995) Different subdomains are most protected from hydrogen exchange in the molten globule and native states of human alpha-lactalbumin. *J. Mol. Biol. 253*, 651–657.
58. Myers, J. K., Pace, C. N., and Scholtz, J. M. (1995) Denaturant m values and heat capacity changes: relation to changes in accessible surface areas of protein unfolding. *Protein Sci. 4*, 2138–2148.
59. Pace, C. N. (1986) Determination and analysis of urea and guanidine hydrochloride denaturation curves. *Methods Enzymol. 131*, 266–280.
60. Pace, C. N., and Scholtz, J. M. (1979) Measuring the conformational stability of a protein. *Biochim. Biophys. Acta* 327–338.
61. Elwell, M. L., and Schellman, J. A. (1979) Stability of phage T4 lysozymes. II. Unfolding with guanidinium chloride. *Biochim. Biophys. Acta 580*, 327–338.
62. Radford, S. E., Buck, M., Topping, K. D., Dobson, C. M., and Evans, P. A. (1992) Hydrogen exchange in native and denatured states of hen egg-white lysozyme. *Proteins 14*, 237–248.
63. Georlette, D., Blaise, V., Collins, T., D'Amico, S., Gratia, E., Hoyoux, A., Marx, J. C., Sonan, G., Feller, G., and Gerday, C. (2004) Some like it cold: biocatalysis at low temperatures. *FEMS Microbiol. Rev. 28*, 25–42.
64. Fink, A. L. (1995) Compact intermediate states in protein folding. *Annu. Rev. Biophys. Biomol. Struct. 24*, 495–522.
65. Redfield, C. (2004) Using nuclear magnetic resonance spectroscopy to study molten globule states of proteins. *Methods 34*, 121–132.
66. Oliveberg, M. (1998) Alternative explanations for "multistate" kinetics in protein folding: transient aggregation and changing transition-state ensembles. *Acc. Chem. Res. 31*, 765–772.
67. Kotik, M., Radford, S. E., and Dobson, C. M. (1995) Comparison of the refolding of hen lysozyme from dimethyl sulfoxide and guanidinium chloride. *Biochemistry 34*, 1714–1724.
68. Wildegger, G., and Kiefhaber, T. (1997) Three-state model for lysozyme folding: triangular folding mechanism with an energetically trapped intermediate. *J. Mol. Biol. 270*, 294–304.
69. Radford, S. E., and Dobson, C. M. (1995) Insights into protein folding using physical techniques: studies of lysozyme and alpha-lactalbumin. *Philos. Trans. R. Soc. London, Ser. B: Biol. Sci. 348*, 17–25.
70. Kulkarni, S. K., Ashcroft, A. E., Carey, M., Masselos, D., Robinson, C. V., and Radford, S. E. (1999) A near-native state on the slow refolding pathway of hen lysozyme. *Protein Sci. 8*, 35–44.